

Shock Tube Size Considerations for Headborne Personal Protective Equipment: A Computational Sensitivity Study

M. Baker¹, R. Kumar¹, V. Alphonse¹, Q. Luong¹, D. Drewry¹, A. Iwaskiw¹

¹The Johns Hopkins Applied Physics Laboratory, 11100 Johns Hopkins Road, Laurel, Maryland 20723, Alexander.iwaskiw@JHUAPL.edu

Abstract: The study of blast-induced traumatic brain injury is becoming increasingly important to the design, manufacturing, and evaluation of headborne personal protective equipment (PPE). Existing testing methodologies rely either on live-fire testing or by recreating blasts using shock tubes to evaluate the blast overpressure attenuating performance of PPE. Previous studies have indicated that shock tube testing can introduce undesired anomalies when compared to live-fire testing [1, 2]. However, specific implications of the size and placement of the test article within shock tubes has seen less focus in literature [3, 4]. Due to the unique size and geometries of headborne PPE, it is important to elucidate both fundamental relationships between testing conditions and blast overpressure loading as well as testing effects of current shock tube systems.

This paper investigates how shock tube and test article size influences the blast overpressure loading using a computational fluid dynamics (CFD) analysis. The investigation used simplified geometries and dimensions to obtain fundamental relationships between geometry and blast overpressure loading. The study used a two-dimensional simulation that independently varied the shock tube cross-sectional dimensions and the circular test article size. The relationships between the shock tube sizes and test articles are comparable to similar shock tube and headform geometries seen in research [2, 5, 6, 7] and can be used to estimate realistic testing effects. Time histories of the blast overpressure signature were evaluated across all simulations. With these data, relationships can be developed and applied to the testing of various headborne PPE geometries to ensure that testing conditions are well understood. Ultimately, these data will inform standards for testing and evaluating PPE appropriately within various shock tube geometries and with a variety of headborne PPE sizes and shapes.

1. INTRODUCTION

Injuries due to blast are a sustained concern for the warfighter. A particularly insidious injury induced by blast, traumatic brain injury, has been observed in recent conflicts and projects to continue to be prevalent in combat [8]. Helmets and other headborne personal protective equipment (PPE) such as goggles, visors and face shields are potentially a very important tool in protecting the warfighter to these types of injuries. Currently there is no standard for evaluating blast-attenuating performance of headborne PPE [6], however progress is being made in developing a standard by utilizing laboratories employing shock tubes. These shock tubes re-create blast waves or shocks seen in live-fire for use in a repeatable testing evaluation methodology. Shock tubes have been known to create undesirable anomalies with respect to a live-fire blast, such as non-uniform shock waves, enhanced impulse exposure, and exit jet gassing. These anomalies have been studied using computation fluid dynamic (CFD) models and mitigation strategies have been integrated into the designs of newer shock tubes, such as tailoring shock generation through adjusting transition regions, changing gas composition for gas-driven shock tubes, and ensuring test articles are placed inside the tube vs outside [1]. While work has been done to generate a shock wave similar to live-fire, very few studies have been conducted to understand the implications of test article size with respect to shock tube size and its influence on testing and evaluation. There have been studies that have indicated that blockage ratio may play a role on pressure loading to a test article [3, 4] however there has not been a study to understand the factors that influence differences in pressure loading in a shock tube. With current geometrical constraints in place with existing shock tubes [2, 5, 6, 7] and headborne PPE, this study aims to evaluate the relationship between blockage ratio and other key metrics associated with pressure loading using CFD modeling. This CFD study spans realistic testing geometries using a simplified two-dimensional (2D) model (circle in a rectangular test region) to understand the effects of shock tube size with respect to test article size.

2. METHODS

2.1 Model selection and setup

Typically, the computational modeling of shock tube testing follows two potential approaches; 1) Fluid-structure interaction (FSI) which models the transient state of the solid test article using the finite element method (FEM) and models the aerodynamics using the finite volume method (FVM), often with reduced complexity to improve numerical stability, or 2) computational fluid dynamics (CFD) modeling which uses the FVM to perform complex modeling of the fluid dynamics and steady-state modeling of the solid test article. The former has the benefit of transient modeling of the fluid-structure interaction, which can predict test article kinematics and deformation – a desire for those interested in momentum transfer due to the shock front. The latter, while only being able to capture the steady-state of the test article, has a higher level of fidelity in the flow solution, and can capture more complex effects such as viscous drag on the test article. This analysis fundamentally is seeking to determine if the chosen metrics, which are derived from the dimensions of the shock tube and test article, can be used to properly describe a robust test configuration. Due to the lack of a need for kinematic results, and a particular interest in the shock wave interactions with the article and tube, a CFD-based analysis approach was chosen. The commercial solver *CFD++* from Metacomp Technologies was used for analysis as it has been validated against previous shock tube testing at the Johns Hopkins Applied Physics Laboratory (JHU/APL), and is sufficiently high fidelity for this analysis [1].

To prepare cases for simulation, a spatial representation (i.e. 2D grid consisting of connected nodes) of a shock tube was developed. Previous analysis leveraged the geometry of the advanced blast simulator at JHU/APL, the Blast Overpressure Simulation System (BOSS), to create a 2D shock tube simulation which would capture the driver and driven regions of the shock tube exactly through a 2D “slice” of the shock tube [1]. The grids used by this paper were simplifications of 2D grids used for the previous analysis and allowed for more specific tuning of the shock tube geometry to match the desired modeling conditions. Figure 18 contains images of these two grids. The simplifications include removing the driver and expansion region of the driven section used by the 2D BOSS model, and replacing them with a single high-pressure region upstream of the test section. As the simulation runs, the high-pressure regions results in a normal shock which arrives at the test article with a similar structure as the one present in the 2D BOSS model. This methodology was chosen to simplify the grid generation process, as varying the expansion region geometry to match the desired blockage ratio could impact the equivalence of the simplified grids. The decision to make these simplifications relies on the assumption that the simplified grid geometry can generate a similar shock at the test article to the 2D BOSS grid. To test this assumption, similar initial conditions were run for both shock tube configurations and the resultant shocks were compared. Both were shown to be planar and had similar overpressure signatures and wave durations.

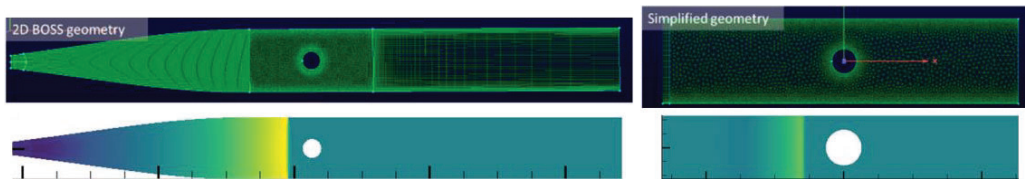


Figure 18. 2D BOSS shock tube geometry (Left) alongside the Simplified shock tube geometry (Right) and comparisons of 2D BOSS grid and simplified grid shock development

The simulation setup consists of 15,000 timesteps of 10^{-6} seconds each. This results in a simulation that models 15 milliseconds of flow, which is consistent with the timescale needed to run a full-scale BOSS shock tube test. All boundaries were treated as adiabatic walls with wall functions used to calculate values at the surface of the test article and tube walls. All flow solutions consider the viscous component of the flow, and the $k-\epsilon$ turbulence model was used. Finally, to match the conditions used in JHU/APL testing campaigns, the simulation was run using air as the fluid of choice.

2.2 Simulation test design

The purpose of this analysis was to leverage 2D CFD to determine if test article size and shock tube size influence the capability of shock tube configurations to simulate free-field blast profiles. To conform to the previous literature on shock tube test validation [1], it was important to consider blockage ratio to

describe the test configuration. Blockage ratio in the context of this analysis refers to the blockage of a circle, defined by the radius r , in a square cross section defined by shock tube side length L (Equation 1). Blockage ratio is varied by changing either the size of the test article (fixed tube case) or changing the width of the simplified shock tube grid (fixed article case) (Figure 19). In each test suite, one of these two variables was fixed to a representative geometry: in the fixed tube case, the tube width was fixed to 914 mm (the tube width of the BOSS); in the fixed article case, the circle diameter was fixed to 179 mm (an approximation of the cross-sectional area of a headform and large headborne PPE system). Varying these geometries can lead to equivalent blockage ratios, but do not necessarily lead to equivalent distances from the test article to the wall. For this reason, the minimum distance to the wall was recorded to identify cases where blockage ratio itself does not fully describe the test configuration (Equation 2). To create results that are representative to real world shock tube test configurations, shock tubes sizes seen in literature tubes [2, 5, 6, 7] were used. In addition to modeling those tube geometries, the bounds of the analysis were extended to capture both low and extremely high blockage cases.

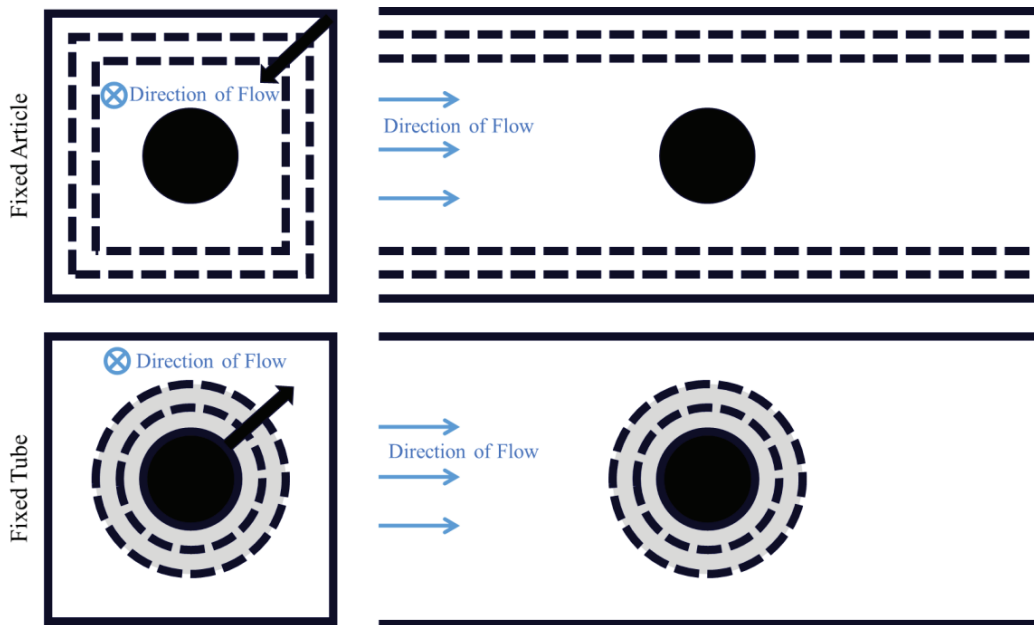


Figure 19. Depiction of the fixed article and fixed tube cases

$$\text{Blockage Ratio} = \frac{\pi r^2}{L^2} \quad (1)$$

$$\text{Minimum distance to the wall} = \frac{L}{2} - r \quad (2)$$

2.3 Data processing steps

The primary variable of interest from the CFD analysis is the pressure at the surface of the test article. The pressure recorded is the static pressure of the flowfield surrounding the article interpolated to the surface of the test article. The point where pressure is recorded is defined by the grid as described in section 2.1, where nodes act as “sensors” recording the simulation data at that specific point on the test article. The sensor locations were at 0° , 45° , and 90° degrees which provided potential for understanding the influence of distance to the wall to the sensor pressure measurement. Additionally, headforms used in headborne PPE testing typically have many sensors placed on the front hemisphere, locations selected in this study approximated these headform locations [6]. The pressure data at the surface is recorded at every timestep of the simulation, allowing the reconstruction of the full overpressure signature of the shock front on the test article. In addition to the pressure at the surface of the test article, the flowfield pressure, velocity, density, and temperature was recorded every 50 timesteps. These data are used to visualise the shock wave development within the shock tube to ensure it is normal, planar, and is traveling

at an appropriate speed when compared to real world shock tube experiments. To record the article surface data, the 'data on boundaries' option in *CFD++* was used. This option allows for the user to extract pressure data at the surface of the test article at every timestep of the simulation.

In free-field blast test conditions, which can be created in live-fire testing, the structure of the blast overpressure at some distance from the blast source can be modeled as a Friedlander wave. The resulting Friedlander wave structure achieved in an empty shock tube is presented in Figure 20 beside experimental data obtained in the JHU/APL shock tube.

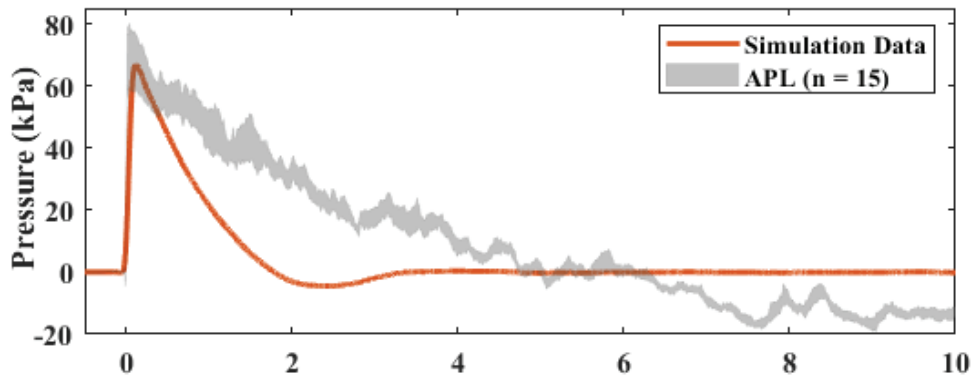


Figure 20. Friedlander wave pressure data from simulation and experimental static pressure response corridor (mean \pm 1 standard deviation) from 15 JHU/APL BOSS measured at the middle of the tube

The data collected is used to inform three main metrics that describe the effect of the shock on the test article: peak overpressure, positive phase duration, and impulse. Peak overpressure is determined by recording the pressure at every timestep of the simulation, subtracting from the pressure readings the standard atmospheric pressure, and determining the first point where the pressure was greater than zero (i.e. greater than standard atmospheric pressure). Positive phase duration is calculated by determining the first point after the peak overpressure is measured where the pressure returns to standard atmospheric conditions. Finally, positive phase impulse is calculated as the integral over time of the pressure acting on the sensor points of interest on the circular test article. This calculation was performed numerically during the post-processing of the computational results. Ten milliseconds of pressure data after the time of shock wave arrival was analyzed. The test article was placed in the shock tube such that the harmonic content of the wave would dissipate, leading to stable impulse measurements. After initial observation, it became clear that the reflected shockwave from the tube wall would be an important phenomenon to characterise, as the reflected peak (and subsequent reflections) occurred during the simulation. In order to characterise the extent of this reflected wave and the effects of the test configuration geometry on the test article pressure loading, two additional metrics are introduced: the ratio of peak pressures, and the second peak time of arrival. The ratio of peak pressures computes how strong the secondary shock is in relation to the strength of the initial shock. The second peak time of arrival denotes the amount of time that passed between the arrival of the initial shock and secondary shock. Both of these metrics offer additional insights into the impact both blockage ratio and minimum distance to the wall have on the pressure trace results.

3. RESULTS

The simulated flow characteristics of the shock through the 2D shock tube were produced every 50 timesteps, and were used to generate visual guides of the shock propagating through the shock tube (Figure 21) along with time histories of the static pressure response measured at three locations.

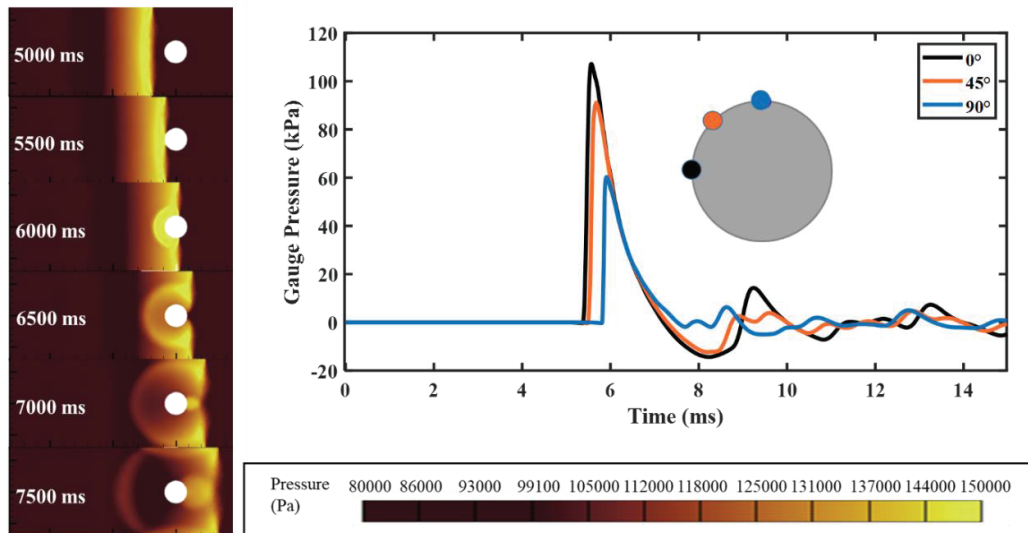


Figure 21. Evolution of blast overpressure for case with 914mm tube length and 116mm test article radius (left) and characteristic time histories of static pressure at 0°, 45° and 90° locations on the test article of a 5% blockage ratio case with a 914mm tube length and a 116mm test article radius (right)

Simulation solutions for low blockage ratio cases showed that the shock impact on the test article did not lead to significant impacts on the planarity and propagation of the shock, as shown in Figure 21. As blockage ratio increases to levels over 30%, a more significant impact on the flow surrounding the test article is observed (Figure 22). These impacts on the flow subsequently impact the recorded ratio of peak pressures, time of arrival of the secondary peak, and impulse experienced by the test article.

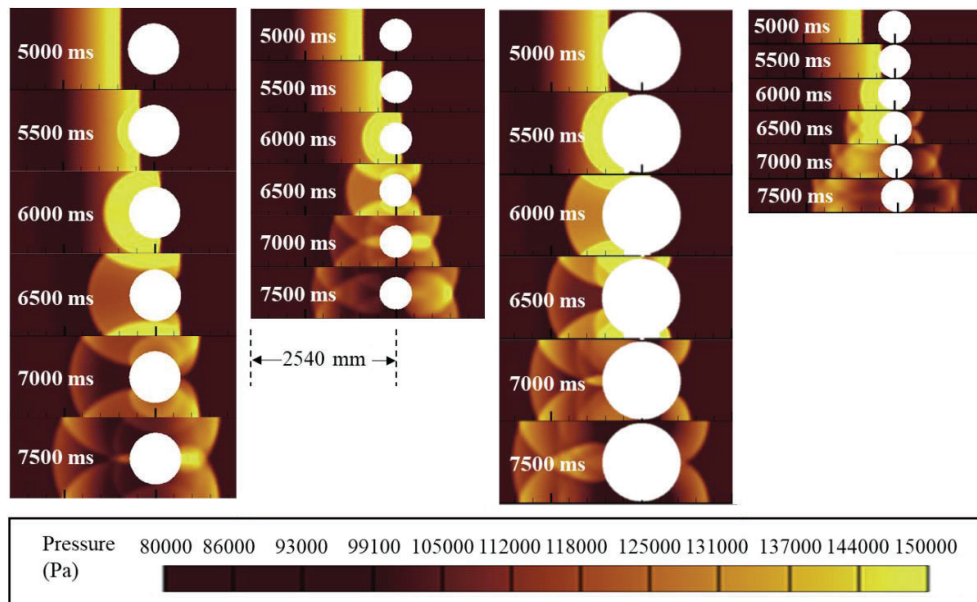


Figure 22. Evolution of blast overpressure for (left to right) 30% blockage ratio fixed tube case (with 914mm tube length and 283mm test article radius), 30% blockage ratio fixed article case (with 579mm tube length and 179mm test article radius), 70% blockage ratio fixed tube case (with 914mm tube length and 432mm test article radius), and 70% blockage ratio fixed article case (with 379mm tube length and 179mm test article radius). Plots of test article and tubes have consistent relative sizes with respect to one another.

Across both cases, an increase in the sensor angle leads to smaller impulse values. This trend holds until both blockage ratio and sensor angle are large, at which point simulation solutions become erratic. Additionally, for both fixed tube (Table 7) and fixed article (Table 8) cases it is observed that as

blockage ratio increases the secondary peak time of arrival shortens significantly, even for the 0° sensor location. Relationships between the blockage ratio and impulse, for cases where both tube size and test article size are held constant, show nonlinear trends at higher blockage ratios (Figure 23) and deviations occur between fixed article and fixed tube cases.

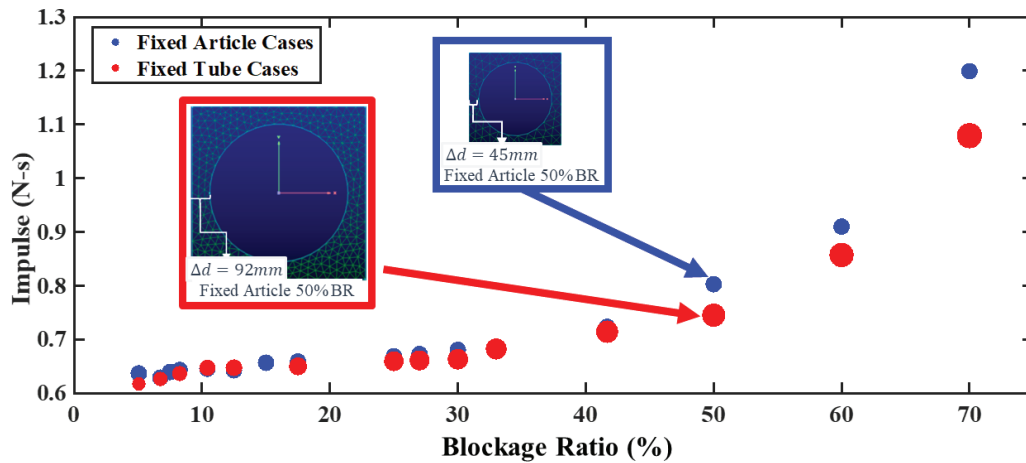


Figure 23. Relationship between blockage ratio and impulse (N-s). Size of circle marker correlates to test article size

Table 7. Fixed tube test matrix and results for 0°, 45°, and 90° sensor locations (omitted data represents anomalous data due to errors in the automated metric selection)

Run	Tube side length (mm)	Radius of the test article (mm)	Blockage Ratio %	Min Dist. To Wall (mm)	Second Peak Time of Arrival (ms)	Ratio of Peak Pressures	Impulse (N-s)	Second Peak Time of Arrival (ms)	Ratio of Peak Pressures	Impulse (N-s)	Second Peak Time of Arrival (ms)	Ratio of Peak Pressures	Impulse (N-s)
					0° sensor location			45° sensor location			90° sensor location		
1	914	116	5.1%	341	2.38	5.9%	0.75	2.10	7.2%	0.62	1.78	26.5%	0.43
2	914	134	6.8%	323	2.36	4.7%	0.76	2.00	6.0%	0.63	1.63	27.9%	0.45
3	914	148	8.3%	309	2.35	5.1%	0.75	1.96	8.2%	0.64	1.58	25.2%	0.44
4	914	167	10.4%	291	2.33	6.7%	0.76	1.89	10.5%	0.65	1.46	28.0%	0.44
5	914	182	12.5%	275	2.31	8.0%	0.77	1.84	13.8%	0.65	1.36	35.8%	0.45
6	914	216	17.5%	241	2.27	10.7%	0.8	1.70	20.1%	0.65	1.14	49.0%	0.46
7	914	258	25.0%	199	2.22	14.3%	0.81	1.53	29.5%	0.66	0.85	71.3%	0.47
8	914	268	27.0%	189	2.20	15.2%	0.82	1.51	29.8%	0.66	0.80	74.7%	0.48
9	914	283	30.0%	175	2.18	16.9%	0.82	1.44	38.1%	0.66	0.71	89.3%	0.48
10	914	296	33.0%	161	2.17	15.9%	0.82	1.38	35.1%	0.68	0.65	84.6%	0.47
11	914	333	42.0%	124	2.12	19.2%	0.84	1.25	46.3%	0.71	0.43	110.7%	0.47
12	914	365	50.0%	92	2.07	21.6%	0.86	1.12	56.5%	0.75	0.27	125.8%	0.43
13	914	400	60.0%	58	2.03	24.4%	0.96	1.01	68.1%	0.86	0.15	84.9%	0.29
14	914	432	70.0%	26	1.99	25.9%	1.16	0.88	78.3%	1.08	0.12	93.1%	

Table 8. Fixed article test matrix and results for 0°, 45°, and 90° sensor locations (omitted data represents anomalous data due to errors in the automated metric selection)

Run	Tube side length (mm)	Radius of the test article (mm)	Blockage Ratio %	Min Dist. To Wall (mm)	Second Peak Time of Arrival (ms)	Ratio of Peak Pressures	Impulse (N-s)	Second Peak Time of Arrival (ms)	Ratio of Peak Pressures	Impulse (N-s)	Second Peak Time of Arrival (ms)	Ratio of Peak Pressures	Impulse (N-s)
					0° sensor location			45° sensor location			90° sensor location		
15	1411	179	5.1%	526	3.68	13.4%	0.78	3.20	2.8%	0.64	2.72	10.5%	0.78
16	1222	179	6.8%	432	3.20	5.6%	0.77	2.68	0.0%	0.63	2.21	20.5%	0.77

17	1159	179	7.5%	400	3.00	3.2%	0.77	2.50	0.0%	0.64	2.04	22.7%	0.77
18	1105	179	8.3%	373	2.83	2.4%	0.78	2.34	1.3%	0.64	1.92	22.8%	0.78
19	983	179	10.4%	313	2.49	4.4%	0.79	2.00	8.5%	0.65	1.55	28.6%	0.79
20	898	179	12.5%	270	2.25	8.6%	0.77	1.76	15.8%	0.64	1.32	36.1%	0.77
21	820	179	15.0%	231	2.04	13.5%	0.79	1.55	22.0%	0.66	1.09	48.5%	0.79
22	759	179	17.5%	200	1.88	18.0%	0.79	1.41	29.0%	0.66	0.94	56.2%	0.79
23	635	179	25.0%	138	1.55	26.9%	0.8	1.08	43.3%	0.67	0.61	78.3%	0.42
24	611	179	27.0%	126	1.49	29.8%	0.81	1.02	46.6%	0.67	0.55	82.7%	0.4
25	579	179	30.0%	111	1.40	36.1%	0.81	0.92	58.1%	0.68	0.46	98.7%	0.38
26	553	179	33.0%	97	1.32	32.8%	0.81	0.85	52.3%	0.68	0.38	92.2%	0.36
27	492	179	42.0%	67	1.16	44.7%	0.85	0.68	71.7%	0.72	0.25	119.0%	0.26
28	449	179	50.0%	45	1.02	50.3%	0.92	0.56	84.0%	0.8	0.11	72.0%	0.13
29	410	179	60.0%	26	0.92	56.5%	1.00	0.46	96.58%	0.9	0.12	96.0%	
30	379	179	70.0%	11	0.84	63.1%	1.23	0.37	104.0%	1.2	0.11	96.6%	0.08

4. DISCUSSION

4.1 Dominant pressure loading mechanism

The results of this study highlight key factors that affect pressure loading in shock tubes. Ritzel [7] considers two main mechanics when discussing short-duration moderate-magnitude (e.g. 200 kPa total pressure) shock waves causing blast-induced motion, which for the purposes of this study, can be a downstream result of pressure loading. These mechanisms are shock wave loading during the diffraction phase and drag loading during shock wave after-flow (or “blast wind”). Ritzel has determined that when a blast wavelength approaches the characteristic length (e.g. diameter of a sphere) that the diffraction phase dominates and there is little to no after-flow over the structure as the shock wave decays very rapidly, reducing the effects of both viscous and form drag loading. In this study, due to the blast wave length of roughly 2 meters, and test article diameters of 0.23-0.86 m, the assumption that there is no drag loading could not be made, however it is expected to be low with respect to the reflected shock pressure loading. When observing the pressure loading of the test article at 30% blockage, it can be seen that secondary shock waves reflect off of the shock tube walls and impart an additional pressure load on the test article while the original primary wave is still loading the test article (Figure 22). Complex wave superposition of test article and wall reflections can be observed creating high pressure loading regions after the wave has passed.

Higher blockage ratios show reflections that prevent a majority of the shock waves from traveling across the test articles (Figure 22). This results in lower pressures seen at the 90° sensor location at higher blockage ratios than the lower blockage ratios. While 70% blockage may be unrealistic for current shock tube designs, this reflection phenomenon may be important when considering test article and article placement in the shock tube as proximity to the wall may create similar complex reflection and choked flow phenomena.

4.2 Relationship between test article and shock tube sizes on response variables

This study aims to understand the relationship between shock tube dimensions, test article dimensions, and pressure loading. Tube size and test article size can vary independently and both have an effect on test articles in shock tubes. In order to further understand the effects of both variables on pressure loading, a commonly used scaled metric blockage ratio (%) can be evaluated. Equation 1 shows that blockage ratio is a metric derived from second order effects of both tube width and test article radius.

The time of arrival of the second wave, due to reflection, varies from 3.7 ms to 0.1 ms. The earliest a secondary wave arrives is at the 90° sensor location in both of the 70% blockage ratio cases. The latest the secondary wave arrives occurs in the fixed article case with 5% blockage ratio. The time of arrival of the second wave decreases (or occurs faster) as blockage ratio increases. Due to the fact that the shock wave used has a duration of 4 ms (and the experimental shock wave durations are even longer) it is expected that reflections will be present in a recorded pressure at the surface of test articles that are of a relevant size, in real shock tubes, for headborne PPE testing. These reflected waves will be present in the pressure response, so the magnitude of the secondary wave should be understood. The range of ratio of the secondary peak to the first, which is a measure of the potential effect of the second wave, spans 0%-116%. Increasing blockage ratio increases the secondary peak ratio as expected. As minimum distance to the wall decreases the ratio of pressure increases, and is highest in the fixed article cases,

where the tubes are the smallest. For some of these high blockage ratio cases, as well as when more complex test article geometries are considered, the simple relationship between the first and second peak magnitude may be insufficient in understanding the extent of influence of the reflections, so a method that integrates pressure over time, like impulse, could be better at explaining the entire effect.

When evaluating impulse for lower blockage ratios (5%-40%) one can identify a trend that exists in both fixed article and fixed tube cases (Figure 23). This trend implies that for lower blockage ratios, the impact of tube width and test article on the loading experienced by the test article is minimal and roughly linear. Moreover, it points to the validity of using blockage ratio to verify the quality of a shock tube configuration, so long as the blockage ratio is within acceptable bounds. Above 40% there is a larger divergence of impulse where this roughly linear relationship breaks down. For these large blockage ratios, cases with lower minimum distances to the side wall see much higher impulses. This may be due to the fact that reflections dominate this response, driven by the fact that cases with shorter distances to the wall have reflections that arrive sooner. For the case of a 445mm tube vs a 914mm tube (both having similar blockage ratios of 50%) the minimum distance to the wall doubles from 45mm to 92mm. It is recommended that further modeling be performed to fully understand the relationship between test article size and tube size, as describing the appropriateness of a test solely on blockage ratio may be insufficient.

4.3 Sensor location

Sensor location has a direct effect on the pressure loading across blockage ratios. For the 0° and 45° sensor locations, impulse and the ratio of peak pressures increase with increased blockage ratio. For the 90° sensor location, impulse decreases with blockage ratio while first and second peak ratio increases. The later trend resulting from the superposition of wave reflections driven by the low minimum distance to the wall. The decrease in impulse at higher blockage ratios is due to the choked flow phenomenon experienced by high blockage ratio test conditions. In these cases, the shock propagation over the top of the article is severely stifled, or entirely limited, by shocks reflecting off of the test article and shock tube wall.

4.4 Implications to headborne PPE testing and evaluation

When considering this research, it is important to think about how these results would affect headborne PPE testing evaluations and methodology. Previous studies have used classic aerodynamic blockage ratios as guidelines for headborne PPE testing methods. These blockage ratios of 5% may be unrealistic to achieve and are rooted in assumptions of quasi-static flow. These results demonstrate that the wavelengths of the short duration shock waves generated in shock tubes are similar in magnitude with the characteristic lengths of headborne PPE and headforms, so the rules that assume drag from flow are not directly applicable in these testing scenarios. Wortman [4] acknowledged that a less-stringent criteria of 20% blockage ratio was acceptable due to the rapidly decaying nature of these pressures, but a sensitivity study had never been run with relevant geometries typically present in PPE and headform shock tube testing. This study used shock tube sizes spanning 377 mm – 1401 mm, capturing and extending the typical sizes seen in literature (610 mm – 1220 mm from the cited reference tubes). The “fixed tube” case represents the JHU/APL’s 914 mm x 914 mm square advanced blast simulator, with test article radii spanning 116 mm – 432 mm. The “fixed article” cases represent a rather large headborne PPE test condition to depict the worst-case headborne PPE that would be tested in a presently available shock tube.

These results show that shock tube testing with blockage ratios approaching 30%-40%, assuming representative geometries of headborne PPE, may be acceptable with only a 7-16% increase in impulse at the 0° and 45° sensor location. At larger blockage ratios, peak metrics such as impulse and magnitude of the second peak increase more rapidly, showing dramatically corrupted pressure loading, with respect to ideal Friedlander waves, versus the lower blockage ratios. At these large blockage ratio values (greater than 40%) minimum distance to the wall must also be considered as a limiting metric of the test configuration. While in some circumstances 30% - 40% blockage ratio can imply a valid testing configuration, the distances to the wall can play a role in enhanced pressure loading. Special care should be taken to maximise the distance between the test article and the side wall in configurations where blockage ratio alone is not beyond 30-40%. Practically, this means test articles should be placed in the middle of the shock tube, but this is not always possible. Additionally, to capture a more complete view of the loading present on a headform or PPE model, sensors should be placed near the point on the article closest to the wall to capture the reflected shock effects on the model.

4.5 Limitations

There are several limitations of this study. The durations of the shock wave generated in this simulation are less than what JHU/APL normally generates in shock tube experiments (Figure 20). Further work should be done to tune parameters in the simulation to modify the shock wave produced, as this could be used to match other relevant blast overpressure signatures seen in other shock tubes. However, the trends observed in the simulations study are relevant for the experimental conditions used in headborne PPE loading. In longer duration shock waves seen in some experiments, the effects of reflections on test article loading may be enhanced. There is a need to validate these results with headform data. It is recommended to continue to tune the initial conditions to create more representative shock waves for future validation. However, these results from the simplified shock tube simulations compared favorably with the previously validated 2D BOSS shock tube grid presented by Kumar et. al. [1]. This study placed a significant emphasis on understanding the impact the shock front has on the side of the test article closest to the driver section. There are additional wave effects on the opposite side of the test article that were not analysed as part of this study that should be considered in future work.

Additionally, the 2D simulations in this study lack the details of real headborne PPE testing such as facial features, head shape, and a helmet. Three dimensional (3D) simulations with those realistic geometries of a headform, like the JHU/APL Human Surrogate Head Model are recommended [6] to be modeled and compared to experimental data for proper validation. There may be more complex reflections that occur from these realistic 3D geometries as well. Another benefit of these realistic geometries is that a one-to-one comparison can be done between sensors on the headform and sensors in the 3D simulation.

This study applied the FVM as implemented in the commercial CFD solver, CFD++. For headborne PPE testing, the pressure loading will cause the kinematics seen in experimental testing and this is not explicitly modeled. However, by modeling with high fidelity the pressure interactions experienced by the test article, these results could provide reliable suggestions for the testing community as to the effects of these specific geometric conditions. Implementation of only the necessary physics, rather than evaluation using a multi-physics approach such as FSI, enables simulation of more complex fluid dynamics at a lower computational cost per simulation than other validated modeling methods implementing FSI approaches. For the exploration of shock tube design, these approaches may be sufficient; however, this method is limited in its ability to represent the kinematics as a separate response variable in the system. Currently, there are many proposed metrics in literature related to brain injury, including global kinematics-based and tissue deformation-based metrics. As this current model cannot account for the kinematic or deformation response of the test article, they do not directly allow analysis into brain injury, but it can be posited that understanding the changes in pressure loading on headforms during testing is an ideal variable in the evaluation of shock tube test configurations themselves.

5. CONCLUSION

The objectives of this study were to evaluate the relationship between shock tube size, test article size and pressure loading across ranges of relevant geometries in headborne PPE testing. Shock tube size and test article size were varied independently and both had an influence on changes in pressure loading as described by change in impulse, ratio of a peak pressures, and second peak time of arrival. Three locations on the test article were evaluated showing different relationships between the geometric variables and “sensor” locations. It was shown that sensor locations closest to the wall are the most sensitive to changes in blockage ratio. While blockage ratio was a good predictor of pressure loading for low to moderate blockage ratios, at high blockage ratios the minimum distance to the wall had significant impacts in the impulse and pressure responses experienced by the test article. Blockage ratios greater than the often cited 20% maximum recommended by Needham [3] were characterised and could be considered for testing, although blockage ratios above 40% seem to greatly affect the pressure loading. These results can better inform decisions in headborne PPE testing including how to avoid influences on pressure loading from higher blockage ratios or non-centred test articles. Ultimately, these data will help inform standards for testing and evaluating PPE within various shock tube geometries to ensure that blast testing and evaluation can be effectively leveraged to achieve greater research goals.

Acknowledgments

The authors would like to thank PEO Soldier Product Manager Soldier Protective Equipment for sponsoring this effort. Any opinions, findings and conclusions or recommendations expressed in this material are those of the

author(s) and do not necessarily reflect the views of PEO Soldier or the NAVAL SEA SYSTEMS COMMAND (NAVSEA).

References

- [1] R. Kumar and A. Nedungadi, "Using Gas-Driven Shock Tubes to Produce Blast Wave Signatures," *Frontiers in Neurology*, vol. 11, no. 90, 2020.
- [2] A. Sundaramurthy, R. Gupta and N. Chandra, "Design considerations for compression gas driven shock tube to replicate field relevant primary blast condition," *ASME International Mechanical Engineering Congress and Exposition*, vol. 56215, 2013.
- [3] E. Needham, D. Ritzel, G. Rule, S. Wiri and L. Young, "Blast testing issues and TBI: experimental models that lead to wrong conclusions," *Frontiers in Neurology*, vol. 6, no. 72, 2015.
- [4] J. Wortman and R. Lottero, "Comparison of HULL Hydrocode Computations of Shock Tube Blockage Effects on Target Loading for Step Shocks and Rapidly-Decaying Shocks," Ballistic Research Laboratory, Aberdeen Proving Ground, MD, USA, 1982.
- [5] A. Sundaramurthy et al., "A 3-D Finite-Element Minipig Model to Assess Brain Biomechanical Responses to Blast Exposure.," *Frontiers in Bioengineering and Biotechnology*, vol. 9, 2021.
- [6] V. A. Alphonse et al., "Helmet Blast Attenuation Performance," in *Personal Armour Systems Symposium*, 2021.
- [7] D. V. Ritzel et al., "Acceleration from short-duration blast.," *Shock Waves*, vol. 28, no. 1, pp. 101-114, 2018.
- [8] P. Hayward, "Traumatic brain injury: the signature of modern conflicts.," *The Lancet Neurology*, vol. 7, no. 3, pp. 200-201, 2008.